Journal of Materials Chemistry A

PAPER

View Article Online
View Journal | View Issue

Design and synthesis of novel carbazole–spacer–carbazole type conjugated microporous networks for gas storage and separation†

Cite this: J. Mater. Chem. A, 2014, 2, 1877

Shanlin Qiao,[ab] Zhengkun Du[a] and Renqiang Yang*[a]

Two novel conjugated microporous networks, P-1 and P-2, with carbazole–spacer–carbazole topological model structures, were designed and prepared by $FeCl_3$ oxidative coupling polymerization. Monomer m-1 (fluorenone spacer) was modified with a thiophene Grignard to form the fluorenyl tertiary alcohol monomer m-2, and this step can increase the polymerization branches from four to five and incorporate the polar –OH group into the building block. N_2 adsorption isotherms show that, after modification, the Brunauer–Emmett–Teller (BET) surface area of P-2 (1222 $m^2\ g^{-1}$) is two times that of P-1 (611 $m^2\ g^{-1}$), and the total pore volume increases 1.63 times from 0.95 to 1.55 at $P/P_0 = 0.99$. However, the domain pore size (centred at 1.19 nm) and the pore distribution of both networks are not changed. It demonstrates that the domain pore width may be determined by the size of the rigid carbazole–spacer–carbazole backbone, not the degree of crosslinking when the networks were prepared under same polymerization conditions in this system. Hydrogen physisorption isotherms of P-1 and P-2 show that the H_2 storage can be up to 1.05 wt% and 1.66 wt% at 77 K and 1.1 bar, and the isosteric heat is 9.89 kJ mol^{-1} and 10.86 kJ mol^{-1}, respectively. At 273 K and 1.1 bar, the CO_2 uptake capacity of P-2 can be up to 14.5 wt% which is 1.63 times that of P-1 under the same conditions. The H_2 and CO_2 uptake capacities of P-2 are among the highest reported for conjugated microporous networks under similar conditions. The CO_2/CH_4 and CO_2/N_2 selectivity results indicate that P-1 exhibits a slightly higher separation ability than P-2. There is often a trade-off between absolute uptake and selectivity in other microporous organic polymers. Fine design and tailoring the topological structure of the monomer can change the adsorption isosteric enthalpy and optimize the gas uptake performance. The obtained networks with the carbazole–spacer–carbazole rigid backbone show promise for potential use in clean energy applications and the environmental field.

Received 6th October 2013
Accepted 11th November 2013

DOI: 10.1039/c3ta14017b

www.rsc.org/MaterialsA

Published on 11 November 2013. Downloaded on 25/03/2014 00:35:20.

Introduction

The rapid consumption of hydrocarbon fuels has caused the emission of large amounts of greenhouse gas into the atmosphere, for example the concentration of CO_2 in the atmosphere is as high as 392 ppm compared to its preindustrial level of *ca.* 280 ppm, forcing the different environmental agencies to encourage the development of new cost-effective technologies to cope with global warming and some climate change issues.[1] The technique of CO_2 capture and sequestration (CCS) in physical processes and utilizing clean energy sources,[2,3] such as hydrogen,[4,5] are of interest to meet these energy and environmental demands. Microporous organic polymers (MOPs), which are composed of light, non-metallic elements and have large specific surface area, narrow pore size distribution and high chemical and thermal stability, present a small energy penalty and cost for state-of-the-art gas uptake applications. Versatile microporous organic polymers such as covalent organic frameworks (COFs),[6] polymers of intrinsic microporosity (PIMs),[7,8] porous aromatic frameworks (PAFs),[9] hypercrosslinked polymers (HCPs),[10,11] crystalline triazine-based organic frameworks (CTFs),[12,13] and conjugated microporous polymers (CMPs),[14,15] have been shown to exhibit high gas storage and separation capacities.

Conjugated microporous polymers (CMPs) are a new class of porous materials which are prepared by transition metal coupling chemistry, such as palladium-catalyzed Stilling, Suzuki, Sonogashira–Hagihara coupling condensation reactions and other oxide coupling reactions. The unique feature of CMPs is that they combine a stiff porous structure and a conjugated electron system in one bulk material, which has been proved to be invaluable in the fields of gas storage,[16] catalysis,[17] and advanced applications in organic electronics[18]

[a]CAS Key Laboratory of Bio-based Materials, Qingdao Institute of Bioenergy and Bioprocess Technology, Chinese Academy of Sciences, Qingdao 266101, China. E-mail: yangrq@qibebt.ac.cn; Fax: +86 532 80662778; Tel: +86 532 80662700

[b]University of Chinese Academy of Sciences, Beijing 100049, China

† Electronic supplementary information (ESI) available. See DOI: 10.1039/c3ta14017b

Published on 11 November 2013. Downloaded on 25/03/2014 00:35:20.

and luminescent sensors.[19] Carbazole, with its rigid backbone and conjugated electron-rich system, is a suitable candidate for the formation of a porous polymer with permanent porosity and enhanced interaction between specific sorbate molecules and adsorbent; in particular the nitrogen-containing structure can greatly increase the uptake capacity for acidic CO_2.[20]

In this work, two carbazole–spacer–carbazole conjugated networks, P-1 and P-2, were synthesized by straightforward $FeCl_3$ oxidative coupling polymerization at room temperature. This polymerization approach using a single building block without any expensive catalysts and requiring mild conditions offers an economical and easy approach towards the synthesis of conjugated porous networks in high yield. In monomer m-1, the carbonyl group of fluorenone was reacted with 2-thienylmagnesium bromide to form the fluorenyl tertiary alcohol monomer m-2. After the polymerization process the two networks will have the same carbazole–spacer–carbazole backbone.[21] The integration of a thiophene unit into the main structure can increase the polymerization branches from four to five, and the α-electron rich position of thiophene also can improve the degree of crosslinking through the high oxidative coupling reactivity. Meanwhile, the carbonyl of fluorenone was converted into a tertiary alcohol group, which is beneficial for CO_2 adsorption. The gas adsorption results show that P-1 and P-2 showed a large difference in porosity structure parameters and gas storage capacity.

Experimental section

Materials

All reagents and solvents, unless otherwise specified, were obtained from J&K, Aldrich and Acros Chemical Co., and were used as received. Anhydrous tetrahydrofuran (THF) and anhydrous chloroform were distilled over sodium/benzophenone and calcium hydride under N_2 prior to use, respectively.

2,7-Bis(*N*-carbazolyl)-9-fluorenone (m-1). A mixture of 2,7-dibromofluoren-9-one (6.72 g, 19.8 mmol), carbazole (7.98 g, 47.7 mmol), K_2CO_3 (16.49 g, 98.0 mmol), CuI (9.09 g, 47.7 mmol), 2,2′-bipyridine (0.005 g) and 1,10-phenanthroline (0.005 g) were dissolved in 1,2-dichlorobenzene (10 mL) under argon protection and shielded from light with tin foil. The mixture was then stirred at 180 °C for 24 h. After the solution cooled to room temperature, the mixture was diluted with CH_2Cl_2 and filtered to remove CuI. The red filtrate was removed by rotary evaporation, and the residue was recrystallized in ethyl acetate to obtain a yellowish solid (5.7 g, 56%). ^{1}H NMR (600 MHz, $CDCl_3$): δ (ppm) = 8.17–8.15 (d, 4H), 7.96 (s, 2H), 7.84–7.83 (d, 2H), 7.78–7.76 (d, 2H), 7.47–7.45 (m, 8H), 7.34–7.32 (m, 4H). ^{13}C NMR (150 MHz, $CDCl_3$): δ (ppm) = 191.85, 142.40, 140.40, 138.96, 136.25, 133.04, 126.23, 123.72, 123.12, 121.85, 120.51, 109.72.

2,7-Di(9*H*-carbazol-9-yl)-9-(thiophen-2-yl)-9*H*-fluoren-9-ol (m-2). m-1 (2.0 g, 3.9 mmol) was dissolved in dry THF (50 mL), and the mixture was slowly added to a Grignard solution prepared from magnesium turnings (0.14 g, 5.9 mmol) reacted with 2-bromothiophene (0.77 g, 4.7 mmol) in dry THF (30 mL). After the addition was completed, the reaction was refluxed overnight. The resulting solution was cooled down to room temperature and quenched with saturated NH_4Cl. After the solution was stirred for 30 min, it was extracted with CH_2Cl_2. The combined extracts were dried over anhydrous $MgSO_4$, the solvent was removed by rotary evaporation, and the residue was purified by column chromatography (petroleum ether–dichloromethane, 3 : 1) to give the pale brownish solid m-2 (1.7 g, 75%). ^{1}H NMR (600 MHz, $CDCl_3$): δ (ppm) = 8.16–8.15 (d, 4H), 7.94–7.93 (d, 2H), 7.86 (s, 2H), 7.68–7.67 (d, 2H), 7.47–7.42 (m, 8H), 7.32–7.30 (t, 4H), 6.97–6.96 (d, 1H), 6.93–6.91 (t, 1H), 2.91 (s, 1H). ^{13}C NMR (150 MHz, $CDCl_3$): δ (ppm) = 151.16, 146.49, 140.65, 137.95, 137.36, 128.31, 126.81, 126.09, 125.60, 124.66, 123.64, 123.55, 121.61, 120.41, 120.21, 109.79, 82.03.

Network of P-1. The solution of monomer m-1 (200 mg, 0.48 mmol) dissolved in 30 mL of anhydrous chloroform was transferred dropwise to a suspension of ferric chloride (648 mg, 3.84 mmol) in 20 mL of anhydrous chloroform. The solution mixture was stirred for 24 h at room temperature under nitrogen protection, and then 100 mL of methanol was added to the above reaction mixture. The resulting precipitate was collected by filtration and washed with methanol and concentrated hydrochloric acid solution. After extraction in a Soxhlet extractor with methanol for 24 h, and then with THF for another 24 h extraction, the desired polymer was collected (red powder, 95% yield) and dried in a vacuum oven at 80 °C overnight. Calcd. C 87.04, N 5.49, H 4.34, O 3.13. Found: C 86.20, N 5.25, H 4.04, O 3.26%.

Network of P-2. The same procedure as for the P-1 network gave a brownish powder, yield 90%. Calcd. C 82.2, N 4.41, H 4.41, O 2.69. Found: C 81.6, N 4.42, H 4.17, O 3.05%.

Instrumentation

^{1}H and ^{13}C NMR spectra were recorded on a Bruker AV 600M spectrometer with tetramethylsilane (TMS) as the internal reference. FT-IR spectra were collected in attenuated total reflection (ATR) mode on a Thermo Nicolet 6700 FT-IR spectrometer. Scanning electron microscopy (SEM) was recorded using a Hitachi S-4800 with an acceleration voltage of 3 kV and a working distance of 3.4 mm. Samples were coated on a thin layer of Au before investigation. For the gas adsorption test, the two networks were degassed at 120 °C for 800 min under vacuum before analysis. BET surface areas and pore size distributions of P-1 and P-2 were measured by nitrogen adsorption–desorption at 77 K. H_2 isotherms were measured at 77 K and 87 K up to 1.1 bar. CO_2, CH_4 and N_2 isotherms were measured at 273 K and 298 K up to 1.1 bar. All the gas adsorption isotherms were tested on a Quantachrome Instruments Autosorb-iQ-MP-VP volumetric adsorption analyzer with the same degassing procedure.

Results and discussion

Two carbazole based conjugated networks, P-1 and P-2, were synthesized by straightforward $FeCl_3$ oxidative coupling polymerization at room temperature, as shown in Scheme 1. The rigid conjugated backbone of carbazole–spacer–carbazole is

 This journal is © The Royal Society of Chemistry 2014

Published on 11 November 2013. Downloaded on 25/03/2014 00:35:20.

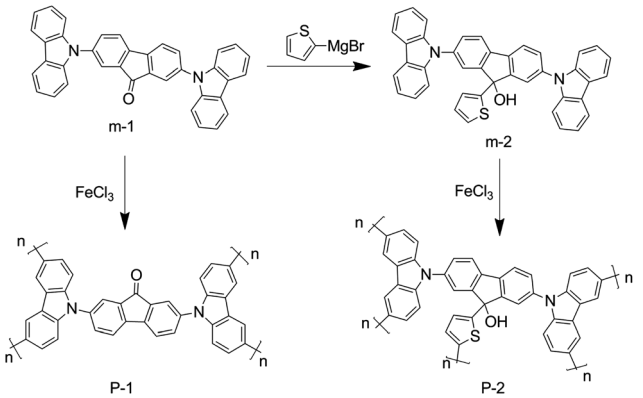

Scheme 1 Synthetic routes towards the networks of P-1 and P-2.

beneficial for the formation of porous networks with permanent porosity stability, and the well-known highly reactive oxidation coupling at the 3,6-position of carbazole makes this backbone a potential building block for the construction of conjugated microporous materials. The monomer m-1 was easily prepared in one step by the Ullmann reaction with one molecule of 2,7-dibromofluoren-9-one and two carbazole units, and the rigid block which is constructed from the three large aromatic units can avoid the pore collapse in the dry state. Carbazole-based fluorenyl tertiary alcohol monomer m-2 was prepared by the Grignard reaction of the ketone substituted by the electron-rich thiophene integrated into fluorenone at the 9 position. The integrated electron-rich thiophene unit at the ketone position not only changes the topological structure of the target polymer (it increases the polymerizing branches, that is, the α-position of thiophene can also undergo oxidative polymerization), but also incorporates an –OH group into the networks, which has previously been shown to lead to improved uptake of CO_2 in MOPs.[22] A more detailed analysis of the structures of the polymers was carried out by FT-IR spectroscopy (Fig. 1a). One can observe that the signal at 1725 cm^{-1} completely disappeared and a signal emerged at 870 cm^{-1} in the spectrum of P-2, which clearly showed that the thiophene unit was successfully integrated into the network. Solid state magic angle spinning ^{13}C CP/MAS NMR spectra and the corresponding networks with assignment of the resonances are shown in Fig. 1b. The characteristic resonance signal peak at 192 ppm corresponds to the carbonyl carbon binding with an oxygen atom (Fig. 1b, bottom). The signal located at 154 ppm is the fluorenyl carbon which is converted by the carbonyl, and the signal at 149 ppm is ascribed to the α-carbon of thiophene binding with the fluorenyl carbon. Thermogravimetric analysis (TGA, Fig. S1†) traces show that P-1 has a higher thermal stability than P-2. The thermal decomposition temperatures (T_d) are up to *ca.* 490 °C for P-1 and 304 °C for P-2 at 5% weight loss. Scanning electron microscopy images (Fig. 1c and d) showed that P-1 and P-2 have similar amorphous aggregated morphologies.

Nitrogen gas sorption analysis

The porosity properties of P-1 and P-2 were measured by adsorption analysis using nitrogen as the probe molecule at

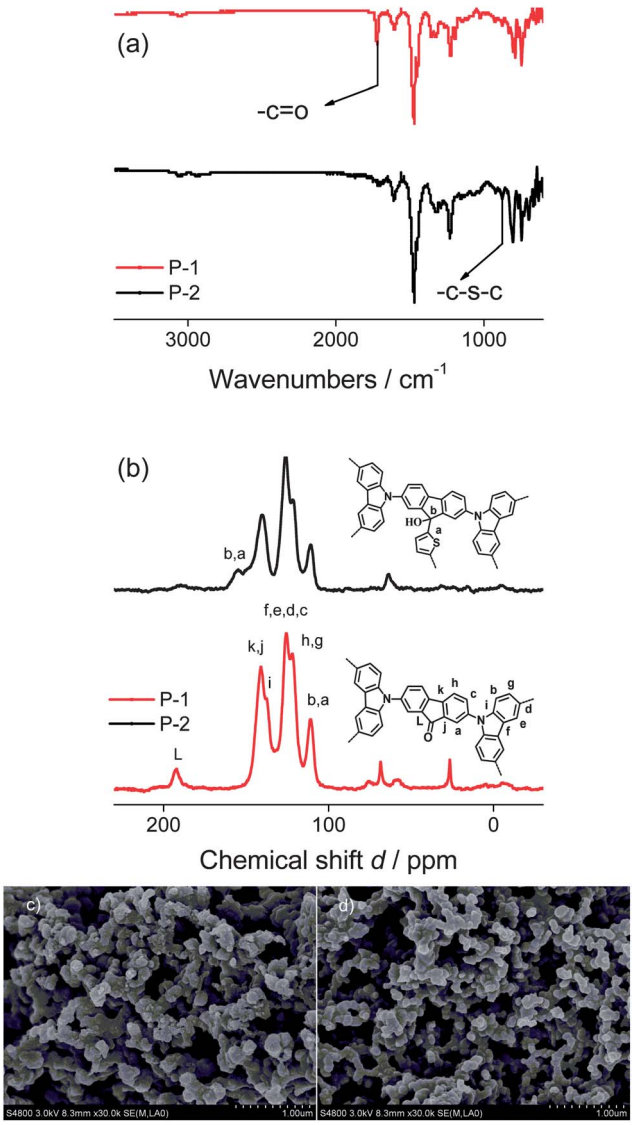

Fig. 1 (a) FT-IR spectra of the P-1 and P-2 networks collected in attenuated total reflection (ATR) mode. (b) Solid state magic angle spinning ^{13}C CP/MAS NMR spectra. (c) P-1 and (d) P-2 field-emission scanning electron microscopy images.

77 K. Fig. 2a shows the N_2 adsorption–desorption isotherms for the two networks. The isotherms demonstrate high gas uptake at relative pressure (P/P_0) less than 0.01, a slowly increasing section at the middle relative pressure range, and a sharp increase in gas adsorption at high relative pressure, indicating significant microporosity and some mesoporosity in the obtained networks. This might be explained by the fact that the mesoporosity arises due to the disorder throughout the structure, leading to some mesopores from linker vacancies.[23] It should be noted that P-2 exhibits an exceptionally high N_2 uptake of 1000 $cm^3\ g^{-1}$ at $P/P_0 = 0.99$. When the Brunauer–Emmett–Teller (BET) model is adopted to calculate the apparent surface area, the values for P-1 and P-2 are 611 $m^2\ g^{-1}$ and 1222 $m^2\ g^{-1}$, respectively. It is interesting that the BET surface area of P-2 is twice that of P-1, when the carbonyl functional

Published on 11 November 2013. Downloaded on 25/03/2014 00:35:20.

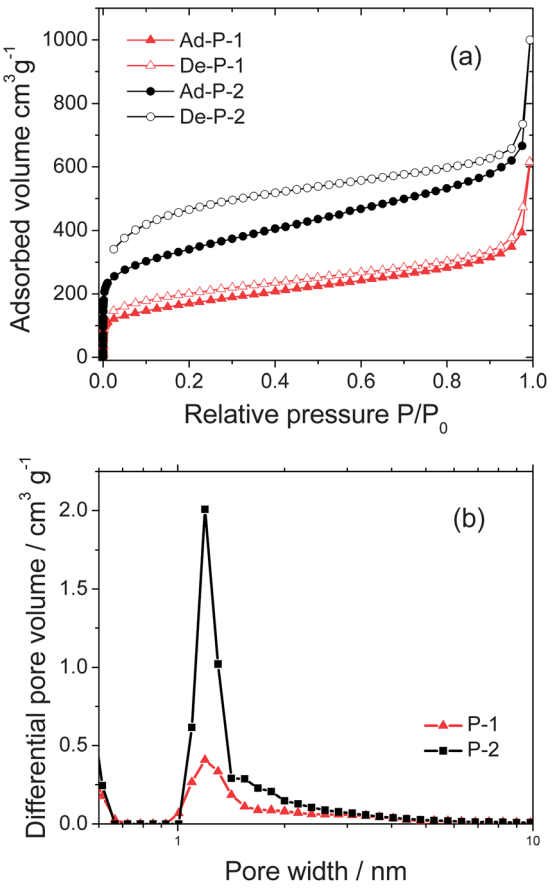

Fig. 2 (a) Nitrogen adsorption–desorption isotherms of the P-1 and P-2 networks measured at 77 K. (b) Pore size distributions calculated using quenched solid density functional theory (QSDFT).

group was modified by a thiophene unit. Conjugated porous materials constructed from other aromatic units have been reported, with BET surface areas for thiophene of 577 $m^2\ g^{-1}$ and 1060 $m^2\ g^{-1}$,[24] spiro-fluorene 450 $m^2\ g^{-1}$[25] and 1000 $m^2\ g^{-1}$,[26] pyrene 505 $m^2\ g^{-1}$,[27] porphyrin 1270 $m^2\ g^{-1}$,[28] and carbazole 2220 $m^2\ g^{-1}$.[29] A large hysteresis in the isotherms is observed for P-2, which is probably because of the existence of metastable state during the gas desorption process, indicative of a swelling efficiency of the polymer matrix resulting from a less rigid thiophene unit introduced into the networks.[30,31] A comparison of pore size distribution (PSD) using quenched solid density functional theory (QSDFT) is shown in Fig. 2b. QSDFT is a multicomponent DFT, in which the networks are treated as one of the components of the adsorbate–adsorbent system. It has been demonstrated that this model can significantly improve the accuracy of pore distribution compared to non-local (NL) DFT.[32] The two networks have the same dominant pore width centred at about 1.19 nm. Integration of the thiophene unit into the monomer m-1 does not change the dominant pore distribution, but increases the pore total volume from 0.95 to 1.55 at relative pressure $P/P_0 = 0.99$. Before the nitrogen adsorption–desorption measurement we inferred that increasing the polymerization branches and changing the topology-directed structure would reduce the dominant pore width of P-2 compared to P-1, however, this prediction was incorrect. The result demonstrated that the dominant pore width was determined by the stiff carbazole–spacer–carbazole backbone, not the polymerization branches in the system. For porous networks, water stability is an important practical consideration. During the post-combustion CO_2 capture process the water vapour is at near-saturation levels, which can accelerate deterioration of the materials used, especially for organic polymers. The water stability of the two networks was assessed as follows. P-1 and P-2 were stirred vigorously in refluxing water in pressure vessels for 24 h. After cooling to room temperature the suspensions were filtered and dried in a vacuum oven at 110 °C overnight, and the samples were named P-1-water and P-2-water. Then, the N_2 adsorption isotherms of P-1-water and P-2-water were measured at 77 K, as shown in Fig. S2†. The BET surface areas of P-1-water and P-2-water were calculated and are listed in parentheses in Table 1. One can observe that, after "cooking" for 24 h in water, the networks have almost the same adsorption curves and BET surface areas as the original networks (Fig. S2,† Table 1). The results indicate that the two networks have good water stability for real applications.

Hydrogen storage

Conjugated microporous polymers with high specific surface area, narrow pore distribution and electron-rich systems are good candidates for gas sorption and storage. Hydrogen physisorption by porous materials is an immensely important topic in clean energy applications. The U. S. Department of Energy (DOE) has set storage targets of 4.5 wt% per 28 g L^{-1} (2010) and 5.5 wt% per 40 g L^{-1} (2015) for hydrogen fuel cell vehicles.[33] The hydrogen physisorption isotherms of the P-1 and P-2 networks were measured at 77 K and 87 K, and are shown in Fig. 3a. In the low pressure range, both networks show a high adsorption amount, suggesting the importance of an electron-rich system for the isosteric heat. This can be easily explained by the electron-rich structure of carbazole–spacer–carbazole backbone. It has been reported that more electric charges on surfaces exhibit strong interactions with H_2 molecules.[34] In the medium pressure range, P-2 shows higher hydrogen uptake than P-1, because P-2 has a higher pore volume than P-1. In this range the pore volume may be the main factor determining hydrogen adsorption capacity. It's worth pointing out that at 77 K and 1.1 bar, P-2 exhibits a H_2 uptake of 1.66 wt%, which is 1.58 times than that of the P-1 network (1.05 wt%). The adsorption curve shows that no saturation will be achieved, indicating that a higher H_2 capacity can be obtained under higher pressure conditions. For hydrogen storage, the optimal pore width at 77 K is considered to be around 10 Å, which is close to where the bulk of the distribution lies in networks P-1 and P-2, and reasonable design and control of the pore width is crucial for hydrogen storage.[35] The H_2 uptake of P-2 is among the highest reported for porous materials, for example, the uptake of polyaniline 0.85 wt%,[36] CMP-2 is 0.91 wt%,[37] PIM-1 is 0.95 wt%,[38] COF-103 is 1.25 wt%,[39] and PPN-3 is 1.58 wt% (ref. 40) under similar conditions. Fig. 3b shows that the P-1 and P-2 networks have isosteric enthalpy (Q_{st})

This journal is © The Royal Society of Chemistry 2014

Published on 11 November 2013. Downloaded on 25/03/2014 00:35:20.

Table 1 Porosity structural parameters of networks P-1 and P-2

Network	S_{BET}[a] ($m^2\ g^{-1}$)	S_{lang} ($m^2\ g^{-1}$)	S_{mic}[c] ($m^2\ g^{-1}$)	V_{mic}[d] ($cm^3\ g^{-1}$)	V_{total}[e] ($cm^3\ g^{-1}$)	Average pore size (Å)
P-1	611 (591)[b]	921	85.7	0.032	0.95	11.9
P-2	1222 (1232)[b]	1451	317	0.135	1.55	11.9

[a] BET surface area calculated based on nitrogen adsorption-branch isotherm in the relative pressure range P/P_0 = 0.07–0.17. BET plots: P-1: correlation coefficient = 0.999995, C constant = 138.523; P-2: correlation coefficient = 0.999989, C constant = 284.453. [b] The BET surface areas were collected after the water stability test (P-1 and P-2 were stirred vigorously in refluxing water in pressure vessels for 24 h). [c] Micropore surface area was calculated using the t-plot method. [d] Microporous volume at P/P_0 = 0.10. [e] Total pore volume at P/P_0 = 0.99.

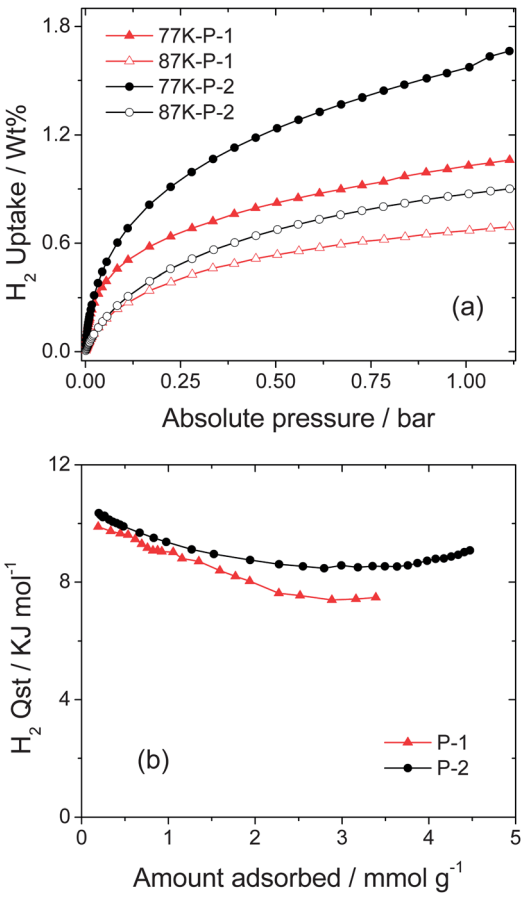

Fig. 3 (a) H_2 adsorption isotherms of P-1 and P-2 networks at 77 K and 87 K. (b) Variation of H_2 isosteric enthalpy with the amount adsorbed.

values of 9.89 kJ mol^{-1} and 10.86 kJ mol^{-1} at zero loading, respectively. This result coincides with the trend of hydrogen adsorption in the low pressure range. It shows that the networks can exhibit strong interactions with H_2 molecules, and thus improve the hydrogen isosteric heat with just the substitution the ketone group by thiophene and a tertiary alcohol unit, rather than changing the backbone of the network.

Carbon dioxide and methane adsorption

To compare the networks of P-1 and thiophene modified P-2 for gas adsorption, CO_2 and CH_4 adsorption isotherms were collected at 273 K and 298 K and pressure up to 1.1 bar, as shown in Fig. 4. The CO_2 physisorption process is reversible in all cases, as the desorption branches are very close to those of adsorption. At 273 K and 1.1 bar, the CO_2 uptake capacity of P-2 can be up to 14.5 wt%, which is 1.63 times greater than the network with fluorenone as the spacer, P-1 (8.9 wt%). It has previously been shown that the incorporation of aromatic thiophene units and alcohol groups into the backbone of networks leads to improved uptake of CO_2 in MOPs.[41] The performance of network P-2 is among the highest among reported MOPs (such as MCTFs: 13.9 wt%,[42] CMP-1: 9.02 wt%,[43] and PECONF-1: 8.2 wt%,[44] at 273 K and 1 bar), and is comparable to other porous materials such as MOFs (ZIF-78: 9.1 wt%,[45] IMFO-3: 8.6 wt%,[46] and MIL-53 (Al): 10.6 wt%[47] at 298 K and 1 bar) under similar conditions. From the adsorption isotherms of CO_2 at 273 K and 298 K, the isosteric enthalpies Q_{st} of polymers P-1 and P-2 are calculated to be 38.8 kJ mol^{-1} and 30.9 kJ mol^{-1} at zero loading based on the Clausius–Clapeyron equation. The P-2 network can retain the same heat of adsorption with increasing quantity of adsorbed CO_2, which enhances the capacity for CO_2 capture despite the relatively modest surface area.[48] The Q_{st} values of the two networks are higher than those of most MOPs, which may be ascribed to the fact that CO_2 is an acidic adsorbate and has a quadrupole moment, which affects the adsorption behaviour on nitrogen-containing and polar modified surfaces; in another words, the adsorption interactions can be strengthened by improving the Lewis-acid and Lewis-base interaction and surface dipole interaction (CO_2: electron-poor adsorbate, polycarbazole: electron-rich adsorbent).[49]

Methane is the main component of natural gas, which is available in large quantities and is environmentally preferable to other hydrocarbons. However, how to use it in a safe and economical way is still a hot topic nowadays. The US Department of Energy (DOE) volumetric storage target for methane is 180 v/v at 35 bar and 298 K.[50] Physisorption of methane onto a support can in principle provide an effective approach for storage with energy densities comparable to compressed gas at much lower pressures. We measured the CH_4 uptake for the two carbazole based networks up to 1.1 bar, as shown in Fig. 4c. The CH_4 uptake of P-1 is 1.35 wt% at 273 K and 0.68 wt% at 298 K, 1.1 bar. The uptake of P-2 is 2.00 wt% at 273 K and 1.17 wt% at 298 K, 1.1 bar. Over the whole pressure range and at both 273 K and 298 K, both networks exhibit steep adsorption isotherms and show no saturation, which means that this type of carbazole-based system can show higher uptake of CH_4 at higher

Published on 11 November 2013. Downloaded on 25/03/2014 00:35:20.

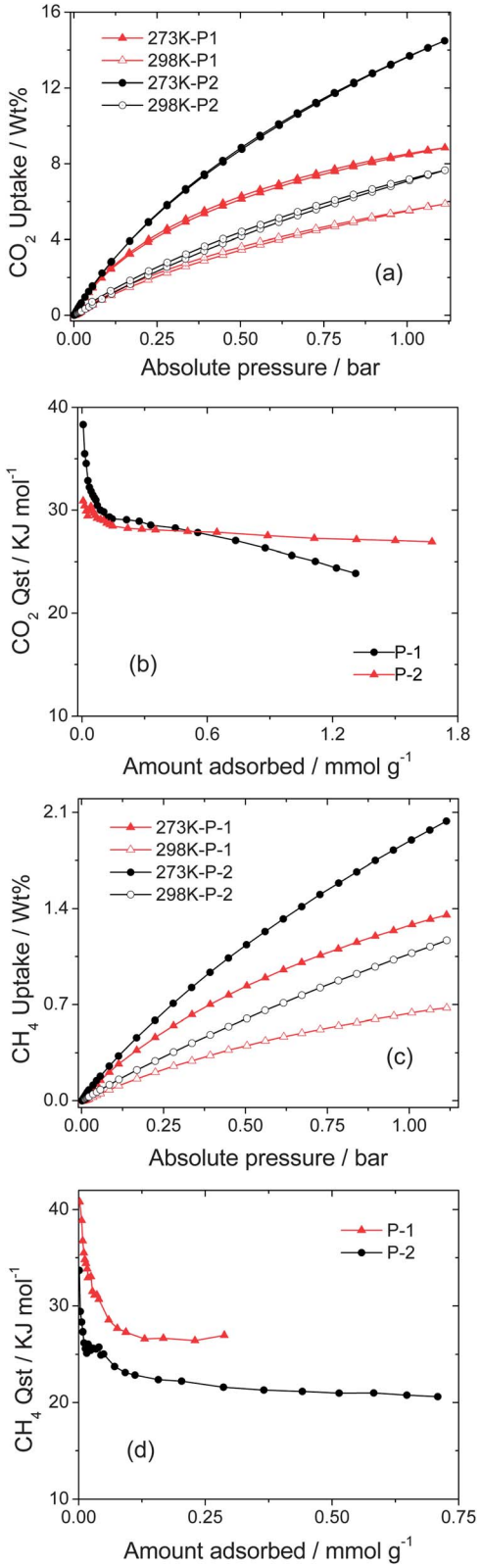

Fig. 4 (a) CO_2 and (c) CH_4 adsorption isotherms of P-1 and P-2 networks at 273 K and 298 K. (b) CO_2 and (d) CH_4 variation of gas isosteric enthalpies with the amount adsorbed.

pressure conditions. It is noteworthy that the isosteric heat of both conjugated networks can be up to 40.81 kJ mol^{-1} and 33.69 kJ mol^{-1} at zero loading, which was calculated from CH_4 adsorption experiments at 273 K and 298 K, respectively (Fig. 4d). The high isosteric heat is advantageous because it allows the possibility of greater storage capacities at lower pressures for materials with comparable micropore size and volume. However, in the low pressure range both isosteric heats fall sharply as the loading increases, and over the whole loading range, the thiophene modified network P-2 shows much lower isosteric heat than that of the fluorenonyl carbazole-based network. This phenomenon is not consistent with the adsorption of H_2 and CO_2 molecules in the two networks. We postulate that this may be due to the lower polarity of the P-1 network combined with the properties of CH_4 molecules, which improve the adsorption interaction between them.

Selectivity of CO_2/CH_4 and CO_2/N_2

The carbazole-based networks of P-1 and P-2 exhibit very different properties for gas storage. In order to deeply understand the relationship between structure and performance, we further investigate the gas selectivity of the two materials for CO_2/CH_4 and CO_2/N_2. Any promising materials for CO_2 capture require not only high CO_2 uptake capacity but also excellent ability for CO_2 selectivity and sequestration. The CO_2/CH_4 and CO_2/N_2 selectivity was estimated using the ratios of the Henry law constants calculated from the initial slopes of the pure component isotherms in the low pressure range, as shown in Fig. 5. The existence of CO_2 reduces the energy density of natural gas. Therefore, separation of CO_2 from a CO_2–CH_4 mixture is very important in industry. The calculated CO_2/CH_4 selectivity of P-1 at 1.1 bar and both 273 K and 298 K is 4.0; the selectivity of P-2 at 1.1 bar and at 273 K and 298 K is 3.0, which is less than that of P-1. One can observe that both networks show stable CO_2/CH_4 selectivity, even if the temperature rises from 273 K to 298 K. The selectivity is higher than that of some reported MOPs, such as PPN-2, PP-3 which show selectivity at low pressure of less than 3. However, the selectivity is lower than that of other porous materials, for example the selectivity of a 2-D MOF with open sites is 13,[51] ZIF-78 is 10,[45] Li-doped 2-Li frameworks is 5 (ref. 52) and zeolite β is 28 (ref. 53) under similar conditions.

Approximately two thirds of CO_2 emissions are generated by the combustion processes in power generation. Capture involves the removal of CO_2 from flue gas which contains a CO_2 concentration of less than 15%.[54] The performance of the two networks for the separation of CO_2/N_2 is shown in Fig. 5. The estimated CO_2/N_2 selectivity of P-1 at 273 K is 18, and P-2 is 16. At 298 K, the selectivity of P-1 is 29 and P-2 is 8, respectively. These selectivity values are comparable to those of COP-1,2 (about 14, 298 K, 1 bar),[55] PPN-6 (7, 295 K),[56] MOF-253 (9, 298 K),[57] and lower than that of NaX zeolite (110, 298 K)[58] under similar conditions.

The separation of CO_2/N_2 was further assessed under more realistic conditions at 313 K, as shown in Fig. S3,† and the selectivity of P-1 is 10 and P-2 is 9. P-1 still exhibits higher

This journal is © The Royal Society of Chemistry 2014

Published on 11 November 2013. Downloaded on 25/03/2014 00:35:20.

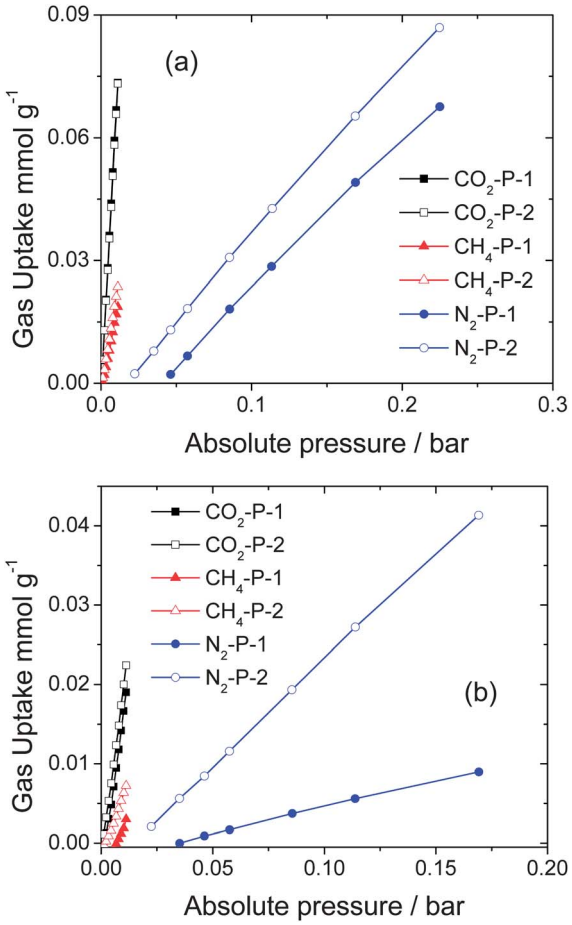

Fig. 5 Initial gas uptake slopes of the two networks for CO_2/CH_4 and CO_2/N_2 at (a) 273 K and (b) 298 K.

selectivity than P-2 despite its much smaller CO_2 uptake compared to P-2. A similar observation can be made for the PECONF series,[59] the BILP series[44] and a series of aniline hypercrosslinked copolymers.[60] There is often a trade-off between absolute uptake and selectivity, and the polymers reported above with the highest CO_2 uptake showed lower selectivity than materials with lower uptakes in this series. It is known that the smaller pore size (pore width <0.7 nm) is advantageous for gas separation. However, in our system both networks have the same backbone and similar domain pore distributions. Thus the pore factor is not the main reason for the difference in gas separation ability. From the microporous data analysis (pore width <2 nm), we inferred that the higher selectivity of P-1 network is most likely due to the significantly higher value of surface area per cubic centimetre (cm^3) of pore volume for P-1 than P-2 (ref. 40) (see Table 1). It is a trade-off that thiophene modified carbazole-spacer-carbazole conjugated networks can increase the CO_2 uptake capacity, but decrease the gas separation efficiency at the same time.

Conclusions

Two rigid carbazole–spacer–carbazole topological type conjugated microporous networks, P-1 and P-2, were designed and prepared by $FeCl_3$ oxidative polymerization. The two networks have the same backbone, monomer m-1 with fluorenonyl as the spacer and m-2 with fluorenyl, respectively. The specific surface areas of P-1 and P-2 are 611 $m^2\ g^{-1}$ and 1222 $m^2\ g^{-1}$, respectively, and the two networks have similar domain pore distributions. This result demonstrated that the domain pore width may be determined by the size of the carbazole–spacer–carbazole rigid backbone. Gravimetric adsorption isotherms show that the adsorption capacity of P-2 for H_2 is 1.66 wt% at 1.1 bar and 77 K, and for CO_2 it is 14.5 wt% at 273 K and 1.1 bar, which are much higher than those of P-1 and among the highest reported for conjugated microporous networks under similar conditions. Further investigation of the CO_2/CH_4 and CO_2/N_2 selectivity shows that P-1 has a slightly higher separation ability than P-2. The obtained networks and their adsorption provide us with an approach to further understand the topological structure design and gas uptake performance for clean energy applications and environmental fields.

Acknowledgements

This work was supported by the National Natural Science Foundation of China (21274161, 51173199), the Ministry of Science and Technology of China (2010DFA52310), the Chinese Academy of Sciences (KGCX2-YW-399+9-2), the Department of Science and Technology of Shandong Province (2010GGC10345), the Shandong Provincial Natural Science Foundation (ZR2011BZ007), and the Qingdao Municipal Science and Technology Program (11-2-4-22-hz).

Notes and references

1 Trends in Atmospheric Carbon Dioxide, U. S. Department of Commerce, National Oceanic & Atmospheric Administration, http://www.esrl.noaa.gov/gmd/ccgg/trends, 2011.
2 R. Dawson, A. I. Cooper and D. J. Adams, *Polym. Int.*, 2013, **62**, 345–352.
3 K. Sumida, D. L. Rogow, J. A. Mason, T. M. McDonald, E. D. Bloch, Z. R. Herm, T. H. Bae and J. R. Long, *Chem. Rev.*, 2012, **112**, 724–781.
4 J. L. C. Rowsell and O. M. Yaghi, *Angew. Chem., Int. Ed.*, 2005, **44**, 4670–4679.
5 L. J. Murray, M. Dinca and J. R. Long, *Chem. Soc. Rev.*, 2009, **38**, 1294–1314.
6 Z. H. Xiang and D. P. Cao, *J. Mater. Chem. A*, 2013, **1**, 2691–2718.
7 N. B. McKeown, B. Gahnem, K. J. Msayib, P. M. Budd, C. E. Tattershall, K. Mahmood, S. Tan, D. Book, H. W. Langmi and A. Walton, *Angew. Chem., Int. Ed.*, 2006, **45**, 1804–1807.
8 N. B. McKeown and P. M. Budd, *Chem. Soc. Rev.*, 2006, **35**, 675–683.
9 T. Ben, H. Ren, S. Ma, D. Cao, J. Lan, X. Jing, W. Wang, J. Xu, F. Deng, J. M. Simmons, S. Qiu and G. Zhu, *Angew. Chem., Int. Ed.*, 2009, **48**, 9457–9460.

Published on 11 November 2013. Downloaded on 25/03/2014 00:35:20.

10 C. D. Wood, B. Tan, A. Trewin, F. Su, M. J. Rosseinsky, D. Bradshaw, Y. Sun, L. Zhou and A. I. Cooper, *Adv. Mater.*, 2008, **20**, 1916–1921.
11 Y. Luo, B. Li, W. Wang, K. Wu and B. Tan, *Adv. Mater.*, 2012, **24**, 5703–5707.
12 P. Kuhn, A. Forget, D. S. Su, A. Thomas and M. Antonietti, *J. Am. Chem. Soc.*, 2008, **130**, 13333–13337.
13 P. Kuhn, M. Antonietti and A. Thomas, *Angew. Chem., Int. Ed.*, 2008, **47**, 3450–3453.
14 A. I. Cooper, *Adv. Mater.*, 2009, **21**, 1291–1295.
15 J. X. Jiang, F. Su, A. Trewin, C. D. Wood, N. L. Campbell, H. Niu, C. Dickinson, A. Y. Ganin, M. J. Rosseinsky, Y. Z. Khimyak and A. I. Cooper, *Angew. Chem., Int. Ed.*, 2007, **46**, 8574–8578.
16 F. Vilela, K. Zhang and M. Antonietti, *Energy Environ. Sci.*, 2012, **5**, 7819–7832.
17 Y. Xie, T. T. Wang, X. H. Liu, K. Zou and W. Q. Deng, *Nat. Commun.*, 2013, **4**, 1960.
18 C. Gu, Y. C. Chen, Z. B. Zhang, S. F. Xue, S. H. Sun, K. Zhang, C. M. Zhong, H. H. Zhang, Y. Y. Pan, Y. Lv, Y. Q. Yang, F. H. Li, S. B. Zhang, F. Huang and Y. G. Ma, *Adv. Mater.*, 2013, **25**, 3443–3448.
19 X. Liu, Y. Xu and D. Jiang, *J. Am. Chem. Soc.*, 2012, **134**, 8738–8741.
20 E. Preis, C. Widling, G. Brunklaus, J. Schmidt, A. Thomas and U. Scherf, *ACS Macro Lett.*, 2013, **2**, 380–383.
21 Z.-D. Liu, Y.-Z. Chang, C.-J. Ou, J.-Y. Lin, L.-H. Xie, C.-R. Yin, M.-D. Yi, Y. Qian, N.-E. Shi and W. Huang, *Polym. Chem.*, 2011, **2**, 2179–2182.
22 X. Zou, H. Ren and G. Zhu, *Chem. Commun.*, 2013, **49**, 3925–3936.
23 P. M. Budd, B. S. Ghanem, S. Makhseed, N. B. McKeown, K. J. Msayib and C. E. Tattershall, *Chem. Commun.*, 2004, 230–231.
24 J. Schmidt, J. Weber, J. D. Epping, M. Antonietti and A. Thomas, *Adv. Mater.*, 2009, **21**, 702–705.
25 J. Weber and A. Thomas, *J. Am. Chem. Soc.*, 2008, **130**, 6334–6335.
26 Q. Chen, J. X. Wang, Q. Wang, N. Bian, Z. H. Li, C. G. Yan and B. H. Han, *Macromolecules*, 2011, **44**, 7987–7993.
27 G. Cheng, T. Hasell, A. Trewin, D. J. Adams and A. I. Cooper, *Angew. Chem., Int. Ed.*, 2012, **51**, 12727–12731.
28 L. Chen, Y. Yang and D. L. Jiang, *J. Am. Chem. Soc.*, 2010, **132**, 9138–9143.
29 Q. Chen, M. Luo, P. Hammershoj, D. Zhou, Y. Han, B. W. Laursen, C. G. Yan and B. H. Han, *J. Am. Chem. Soc.*, 2012, **134**, 6084–6087.
30 N. B. McKeown, P. M. Budd, K. J. Msayib, B. S. Ghanem, H. J. Kingston, C. E. Tattershall, S. Makhseed, K. J. Reynolds and D. Fritsch, *Chem.–Eur. J.*, 2005, **11**, 2610–2620.
31 J. Weber, J. Schmidt, A. Thomas and W. Bohlmann, *Langmuir*, 2010, **26**, 15650–15656.
32 A. V. Neimark, Y. Z. Lin, P. I. Ravikovitch and M. Thommes, *Carbon*, 2009, **47**, 1617–1628.
33 DOE Targets for On-Board Hydrogen Storage Systems for Light-Duty Vehicles, http://www1.eere.energy.gov/hydrogenandfuelcells/storage/pdfs/targets on board hydro storage.pdf.
34 C. D. Wood, B. Tan, A. Trewin, H. Niu, D. Bradshaw, M. J. Rosseinsky, Y. Z. Khimyak, N. L. Campbell, R. Kirk, E. Stoeckel and A. I. Cooper, *Chem. Mater.*, 2007, **19**, 2034–2048.
35 J. A. Alonso, I. Cabria and M. J. Lopez, *J. Mater. Res.*, 2013, **28**, 589–604.
36 J. Germain, F. Svec and J. M. J. Frechet, *Chem. Mater.*, 2008, **20**, 7069–7076.
37 J. X. Jiang, F. Su, A. Trewin, C. D. Wood, H. Niu, J. T. A. Jones, Y. Z. Khimyak and A. I. Cooper, *J. Am. Chem. Soc.*, 2008, **130**, 7710–7720.
38 P. M. Budd, B. S. Ghanem, S. Makhseed, N. B. McKeown, K. J. Msayib and C. E. Tattershall, *Chem. Commun.*, 2004, 230–231.
39 H. Furukawa and O. M. Yaghi, *J. Am. Chem. Soc.*, 2009, **131**, 8875–8883.
40 W. G. Lu, D. Q. Yuan, D. Zhao, C. I. Schilling, O. Plietzsch, T. Muller, S. Brase, J. Guenther, J. Blumel, R. Krishna, Z. Li and H. C. Zhou, *Chem. Mater.*, 2010, **22**, 5964–5972.
41 A. P. Katsoulidis and M. G. Kanatzidis, *Chem. Mater.*, 2011, **23**, 1818–1824.
42 X. Liu, H. Li, Y. Zhang, B. Xu, A. Sigen, H. Xia and Y. Mu, *Polym. Chem.*, 2013, **4**, 2445.
43 R. Dawson, D. J. Adams and A. I. Cooper, *Chem. Sci.*, 2011, **2**, 1173–1177.
44 P. Mohanty, L. D. Kull and K. Landskron, *Nat. Commun.*, 2011, **2**, 401–406.
45 R. Banerjee, H. Furukawa, D. Britt, C. Knobler, M. O'Keeffe and O. M. Yaghi, *J. Am. Chem. Soc.*, 2009, **131**, 3875–3877.
46 F. Debatin, A. Thomas, A. Kelling, N. Hedin, Z. Bacsik, I. Senkovska, S. Kaskel, M. Junginger, H. Muller, U. Schilde, C. Jager, A. Friedrich and H. J. Holdt, *Angew. Chem., Int. Ed.*, 2010, **49**, 1258–1262.
47 B. Arstad, H. Fjellvåg, K. O. Kongshaug, O. Swang and R. Blom, *Adsorption*, 2008, **14**, 755–762.
48 J. R. Holst and A. I. Cooper, *Adv. Mater.*, 2010, **22**, 5212–5216.
49 A. Arenillas, F. Rubiera, J. B. Parra, C. O. Ania and J. J. Pis, *Appl. Surf. Sci.*, 2005, **252**, 619–624.
50 T. Burchell and M. Rogers, *Soc. Automot. Eng. Tech. Pap. Ser.*, 2000, 2000–2205.
51 B. Mu, F. Li and K. S. Walton, *Chem. Commun.*, 2009, 2493–2495.
52 Y. S. Bae, B. G. Hauser, O. K. Farha, J. T. Hupp and R. Q. Snurr, *Microporous Mesoporous Mater.*, 2011, **141**, 231–235.
53 K. K. Tanabe, Z. Q. Wang and S. M. Cohen, *J. Am. Chem. Soc.*, 2008, **130**, 8508–8517.
54 J. A. Mason, K. Sumida, Z. R. Herm, R. Krishna and J. R. Long, *Energy Environ. Sci.*, 2011, **4**, 3030.
55 Z. H. Xiang, X. Zhou, C. H. Zhou, S. Zhong, X. He, C. P. Qin and D. P. Cao, *J. Mater. Chem.*, 2012, **22**, 22663–22669.
56 W. G. Lu, D. Q. Yuan, J. L. Sculley, D. Zhao, R. Krishna and H. C. Zhou, *J. Am. Chem. Soc.*, 2011, **133**, 18126–18129.

 This journal is © The Royal Society of Chemistry 2014

57 E. D. Bloch, D. Britt, C. Lee, C. J. Doonan, F. J. Uribe-Romo, H. Furukawa, J. R. Long and O. M. Yaghi, *J. Am. Chem. Soc.*, 2010, **132**, 14382–14384.
58 Y. Belmabkhout, G. Pirngruber, E. Jolimaitre and A. Methivier, *Adsorption*, 2007, **13**, 341–349.
59 M. G. Rabbani and H. M. El-Kaderi, *Chem. Mater.*, 2012, **24**, 1511–1517.
60 R. Dawson, T. Ratvijitvech, M. Corker, A. Laybourn, Y. Z. Khimyak, A. I. Cooper and D. J. Adams, *Polym. Chem.*, 2012, **3**, 2034–2038.

Published on 11 November 2013. Downloaded on 25/03/2014 00:35:20.